https://doi.org/10.5194/egusphere-2026-1081
Preprint. Discussion started: 4 May 2026

Joint Bayesian Calibration of Frontal Ablation and Surface Mass Balance in Global Glacier Models

Ruitang Yang[1], Lizz Ultee[2,3], Kristoffer Aalstad[1], Matvey V. Debolskiy[1], Regine Hock[1], Patrick Schmitt[4], David Rounce[5], and Tian Li[6]

[1]Department of Geosciences, University of Oslo, Oslo, Norway
[2]NASA Goddard Space Flight Center, Greenbelt, MD, USA
[3]Morgan State University, Baltimore, MD, USA
[4]University of Innsbruck, Innsbruck, Austria
[5]Department of Civil and Environmental Engineering, Carnegie Mellon University, Pittsburgh, PA, USA
[6]Bristol Glaciology Centre, University of Bristol, Bristol, UK

Correspondence: Ruitang Yang (ruitang.yang@geo.uio.no)

Abstract. Modeling frontal ablation of marine-terminating glaciers is critical for accurately modeling mass change but remains challenging. We present a hybrid, physically consistent and numerically efficient modelling framework that integrates the Simple Estimator of Retreat Magnitude and ice flux (SERMeQ) into two coupled global glacier models (OGGM and PyGEM). The adaptive particle-batch smoother, a Bayesian data assimilation method, is used for joint calibration of all parameters. The coupled framework simulates monthly length changes along flowlines and mass-balance components of individual glaciers. Applied to 71 marine-terminating glaciers across Svalbard during the period of 2000-2019, the model simulates distinct seasonal variations and annual length changes of glacier calving fronts, while reproducing decadal climatic mass balance estimates well. However, frontal ablation tends to be overestimated possibly due to uncertainties in initial geometry and modelled ice velocities. Overall, the good alignment of the regional distributions highlights that the modeling framework, including the efficient joint Bayesian calibration, provides a promising tool for large-scale frontal ablation modeling in glacier evolution models.

1 Introduction

Frontal ablation refers to the mass loss due to calving, melting, and sublimation at the near-vertical margins of marine-terminating glaciers (Cogley et al., 2011). Approximately 38% of the total glacier area outside the ice sheets drain directly into the ocean (Gardner et al., 2013) and is subject to frontal ablation. Kochtitzky et al. (2022) estimated that frontal ablation of all marine-terminating glaciers in the northern hemisphere (excluding the Greenland ice sheet) increased from an average of 44.47 $\pm$ 6.23 Gt a^{-1} from 2000 to 2009, to 51.98 $\pm$ 4.62 Gt a^{-1} from 2010 to 2019. Accurately simulating frontal ablation within large-scale glacier evolution models is thus essential for elucidating the dynamics and mass balance of marine-terminating glaciers, thereby enhancing our understanding of their contributions to global sea-level rise in a changing climate (Benn et al., 2007). However, the physical processes involved in frontal ablation (e.g. calving, submarine melting, and ice-ocean interactions) are complex and highly localized, making robust physical parameterization challenging. Scarcity of high-resolution front

https://doi.org/10.5194/egusphere-2026-1081
Preprint. Discussion started: 4 May 2026

observations (thickness, bathymetry, and ocean forcings) combined with difficulties in calibration (noisy data, structural model errors, and parameter non-uniqueness) undermines model validation and limits confidence in simulations (Recinos et al., 2021; Malles et al., 2023).

Reliable modeling approaches are also crucial for quantifying and projecting frontal ablation. Early studies in the 1990s established an empirical linear relationship between calving rates and water depth for marine-terminating glaciers (Brown, 1983; Pelto and Warren, 1991). Subsequent studies proposed physical explanations for this scaling (Hanson and Hooke, 2000), but also demonstrated its limitations during rapid transitions, motivating modified flotation criteria based on height-above-buoyancy (Vieli et al., 2001; van der Veen, 2002). Building on mass conservation principles, minimal conceptual models were developed to link ice thickness and glacier length and thus enable long-term simulations of terminus change (Oerlemans and Nick, 2005). More process-based approaches then incorporated crevasse propagation and penetration physics (with three-dimensional extensions) to capture calving mechanics and seasonal terminus cycles (Benn et al., 2007; Otero et al., 2010; Nick et al., 2010). Finally, unlike the earlier empirical models, yield-criterion–based, numerically efficient flowline schemes such as the Simple Estimator of Retreat Magnitude and Ice Flux (SERMeQ) embed a physically consistent yield criterion in a fast solver, enabling them to produce simultaneous estimates of retreat magnitude and ice flux that reproduce observed terminus advance–retreat patterns (Ultee and Bassis, 2020). A recent study employing a 3D glacier dynamics model for the Hansbreen–Hansbukta system in Svalbard successfully reproduced seasonal calving-front variations but lacked quantitative uncertainty estimates (Muñoz-Hermosilla et al., 2024). However, most existing frontal ablation models either lack sufficient refinement and validation or are computationally too demanding at large-scale or for long-term simulations.

The current generation of global glacier evolution models either omit frontal ablation entirely or parameterize it in a highly simplified fashion (Marzeion et al., 2020). A modified empirical linear relationship between calving rate and water depth (Oerlemans and Nick, 2005) is so far - to our knowledge - the only frontal ablation parameterization used in global glacier models; examples include within the Global Glacier Evolution Model ("GloGEM"; Huss and Hock, 2015), Open Global Glacier Model ("OGGM"; Maussion et al., 2019; Recinos et al., 2019), and Python Glacier Evolution Model ("PyGEM"; Rounce et al., 2023). Although practical, these empirical relationships do not explicitly capture the physical mechanisms of calving.

Model calibration compounds these limitations (Yang et al., 2025). Computationally intensive Markov Chain Monte Carlo (MCMC) methods are commonly applied given the growing availability of remote-sensing and machine-learning datasets (e.g., Murphy, 2023; Rounce et al., 2020b; Sjursen et al., 2025). More efficient ensemble-based data-assimilation methods (Evensen et al., 2022), such as particle filters and other Sequential Monte Carlo techniques (Chopin and Papaspiliopoulos, 2020), can deliver comparable probabilistic inference with far fewer forward runs and greater parallelizability (Aalstad et al., 2026). These approaches are increasingly applied in cryospheric research and in glacier-focused studies (Alonso-González et al., 2022; Landmann et al., 2021; Navari et al., 2021; Cao et al., 2025).

To improve global projections of glacier change and better capture local impacts (e.g., on tourism and ecosystems), more physically based parameterizations of frontal ablation into global glacier models are needed, supported by rigorous calibration and uncertainty quantification. In this study, we present a numerically efficient framework that integrates the physically-based

https://doi.org/10.5194/egusphere-2026-1081
Preprint. Discussion started: 4 May 2026

frontal ablation model SERMeQ into a global glacier mass balance scheme. In addition, we apply a joint Bayesian calibration using an ensemble-based data assimilation method to jointly optimize frontal ablation and climatic mass balance parameters and to quantify uncertainties systematically. The framework is tested on 71 marine-terminating glaciers in Svalbard for both hindcast (2000 - 2019) and future projections (2020 - 2100) under multiple climate scenarios to highlight the utility of the framework for large-scale glacier evolution models.

2 Model framework

Our approach is based on the coupled PyGEM–OGGM hybrid framework by incorporating SERMeQ, each component addressing a distinct aspect of glacier evolution. The climatic mass balance of the glacier is estimated by PyGEM (version 0.2.0 Rounce et al., 2023); glacier dynamics are simulated with OGGM (version 1.6.2 Maussion et al., 2019), which also performs bed inversion; and frontal ablation is calculated based on SERMeQ (Ultee and Bassis, 2020). All three models are "glacier-centric", meaning they simulate the evolution of individual glaciers, and all have been applied at regional and/or global scales. To calibrate model parameters we employ an ensemble-based data assimilation method. The key elements of each component model and the Bayesian calibration method are briefly outlined below; for further details, we refer readers to the relevant model description papers.

2.1 Description of the Integrated Models

2.1.1 PyGEM climatic mass balance model

PyGEM simulates the climatic mass balance for every 10 m elevation bins monthly (Rounce et al., 2023, 2020a) . Melt is computed using a degree-day scheme that accounts for different surface types by using different degree-day factors for snow, ice, and firn surfaces. Snow accumulation is computed as a function of precipitation with a threshold temperature discriminating between solid and liquid precipitation. Refreezing is calculated as a function of mean annual air temperature. Three parameters in PyGEM must be calibrated: the snow degree-day factor f_{snow}, the temperature bias correction T_{bias}, and the precipitation correction factor k_{p}.

2.1.2 OGGM glacier dynamics model

OGGM's ice-flow module simulates glacier dynamics and updates glacier geometry (extent and surface elevation); OGGM is coupled to PyGEM via PyGEM's default framework. OGGM uses the shallow ice approximation, applied along elevation-band flowlines (Marzeion et al., 2012; Maussion et al., 2019). The dynamic scheme solves for the depth-integrated ice velocity u as a function of the basal shear stress τ:

$$u = \left(\frac{2Ah}{n+2} + \frac{f_s}{h} \right) \tau^n \tag{1}$$

where A is Glen's creep parameter, h is ice thickness, f_s a sliding factor, and n a power-law exponent (set to 3 in usual Nye-Glen flow for glaciers). The basal shear stress τ is assumed equal to the gravitational driving stress.

https://doi.org/10.5194/egusphere-2026-1081
Preprint. Discussion started: 4 May 2026

Subsequently, the climatic mass balance from PyGEM and the velocity from OGGM serve as inputs for SERMeQ to determine terminus position change, frontal ablation, and mass flux. The glacier geometry is updated monthly via the flowline model, acting as input for the next time step iteration.

2.1.3 SERMeQ frontal ablation model

Frontal ablation (A_f, defined as positive) is calculated by

$$A_f = (U - \frac{dL}{dt})S_f, \tag{2}$$

in which S_f is the cross-sectional area of the terminus (ice thickness * width), U is the ice speed at the terminus, and $\frac{dL}{dt}$ is the front position change rate along each glacier centerline and solved by SERMeQ (positive for advance, negative for retreat).

SERMeQ simulates the glacier's changing geometry along flowlines using a vertically integrated, bi-viscous rheology (Ultee and Bassis, 2016; Bassis and Ultee, 2019). SERMeQ calibrates a single parameter, the yield strength of ice τ_y, based on observed glacier surface elevation profile. It then evolves the glacier front position and surface elevation profile in response to forcing:

$$\frac{dL}{dt} = \frac{\dot{a} - H\frac{\partial U}{\partial x} - U\frac{\partial H}{\partial x}}{\frac{\partial H_y}{\partial x} - \frac{\partial H}{\partial x}}. \tag{3}$$

In Equation 3, $L = L(t)$ is the front position of the glacier, where all other terms are evaluated; $\dot{a}(x,t)$ is the net ice accumulation rate, $H(x,t)$ is the ice thickness, and $U(x,t)$ is the ice velocity. $H_y(x,\tau_y)$ is the thickness at which effective stress within the ice reaches its yield strength (the "yield thickness"):

$$H_y = 2\frac{\tau_y}{\rho_i g} + \sqrt{\frac{\rho_w}{\rho_i}D^2 + \left(\frac{2\tau_y}{\rho_i g}\right)^2}, \tag{4}$$

where $\rho_i = 920$ kg m^{-3} is the density of glacier ice, $\rho_w = 1020$ kg m^{-3} the density of seawater, $g = 9.81$ m s^{-2} the acceleration due to gravity, and D is the water depth at the glacier terminus.

In standalone mode, SERMeQ solves for the terms in Equation 3 using the shallow ice approximation to Nye-Glen flow and taking surface mass balance input from a regional climate model (Ultee and Bassis, 2020). For coupling with OGGM and PyGEM, we have implemented Equation 3 to evolve the front position in response to ice velocity output by OGGM, leaving all mass balance processes to be handled by coupled PyGEM-OGGM. We also perform a joint calibration of τ_y together with the three climatic mass balance parameters in PyGEM for the coupled case (§2.3).

2.2 Model coupling approach

The coupling framework of PyGEM-OGGM-SERMeQ was designed to align with the modular philosophy of the models while supporting their continuous development. To enable monthly-scale coupling, all models were minimally adapted to ensure seamless integration. The frontal ablation model (SERMeQ) was nested within the flowline model (OGGM), thereby replacing

https://doi.org/10.5194/egusphere-2026-1081
Preprint. Discussion started: 4 May 2026

the previous parameterizations and allowing frontal ablation dynamics to directly influence glacier flow and geometry in real-time during the flowline simulation. To fully capture time-varying terminus changes and the frontal ablation term, geometric update outputs are now generated monthly instead of using OGGM's default annual output. The resulting monthly glacier geometries are then integrated with the climatic mass balance model (PyGEM) and monthly climate data.

The framework follows a nested-sequential iterative coupling structure and operates individually for each glacier. The workflow begins with PyGEM, which calculates the climatic mass balance based on the elevation-band flowline geometry provided by OGGM. The output from PyGEM is passed to OGGM to simulate glacier ice flow. Within each flowline time step, SERMeQ is executed as an embedded subroutine that assesses terminus conditions (e.g., ice thickness, water depth, and yield strength) and computes the resulting change in terminus position and associated frontal ablation. The computed frontal ablation is then passed to OGGM's flowline model, which uses it to update the flowline geometry.

The updated flowline geometry is subsequently passed back to PyGEM for the next time step, where the climatic mass balance is recalculated. This process—climatic mass balance $\longrightarrow$ flowline dynamics $\longrightarrow$ nested frontal ablation $\longrightarrow$ flowline update—is repeated iteratively across time steps to capture the dynamic interplay between surface mass balance, glacier flow, and frontal ablation processes.

2.3 Bayesian calibration based on adaptive particle batch smoother

The Bayesian calibration approach (see details in Supplement section S1) facilitates the quantification of uncertainties for each glacier, presuming that these glacier-specific parameters remain constant over time. To avoid the circularity issue that plagued previous models (Rounce et al., 2023; Malles et al., 2023), we employ a new Bayesian inference via ensemble-based data assimilation to jointly calibrate four model parameters: the snow degree-day factor f_{snow}, the temperature bias correction T_{bias}, and the precipitation correction factor k_{p}, together with the yield strength τ_y. The parameter values are collected in the 4×1 vector. Our framework can readily accommodate additional parameters as required. For the present study we adopt the default values for Glen's creep parameter and the sliding factor, $A = 2.4 \times 10^{-24}\,\text{m}^3\,\text{s}^5\,\text{kg}^{-3}$ and $f_{\text{s}} = 5.7 \times 10^{-20}\,\text{m}^5\,\text{s}^5\,\text{kg}^{-3}$ respectively, which represent glacier motion arising from a combination of ice deformation and sliding over the bed.

We use a robust iterative variant of this scheme known as adaptive particle batch smoother (AdaPBS) described in detail in Aalstad et al. (2026), which has been applied to snow (Aalstad et al., 2026) and permafrost (Willmes et al., 2025) research, and now to glaciers. We utilize a logit-normal distribution (Cao et al., 2025) as the prior distribution for the four parameters, which is informed by physical constraints and expert knowledge. Specifically, this distribution draws on data for mass balance parameters (f_{snow}, k_{p}, T_{bias}) from PyGEM (Rounce et al., 2020b) and yield strength (τ_y) from previous studies (Ultee and Bassis, 2020; O'Neel et al., 2005; Cuffey and Paterson, 2010); see Table 1.

The parameters are assumed conditionally independent a-priori given our probabilistic model, so the joint prior is simply the product of marginal priors $p(\boldsymbol{\theta}) = p(f_{\text{snow}})p(k_{\text{p}})p(T_{\text{bias}})p(\tau_y)$. Note that this does not necessarily imply that the parameters are independent in the posterior $p(\boldsymbol{\theta} \mid \mathbf{y})$, since dependence may enter when conditioning on the data via the likelihood $p(\mathbf{y} \mid \boldsymbol{\theta})$.

The AdaPBS extends the particle batch smoother (Margulis et al., 2015, PBS;) by replacing prior-only sampling with adaptive multiple importance sampling (Cornuet et al., 2012) to update the particle ensemble while preserving full parallelizability.

https://doi.org/10.5194/egusphere-2026-1081
Preprint. Discussion started: 4 May 2026

This is a robust adaptive importance sampling strategy (Bugallo et al., 2017) that reuses the complete particle history, improving sample efficiency for computationally expensive cryospheric models. Unlike the original particle batch smoother, which samples once from the prior and weights particles by their likelihood over the smoothing window, AdaPBS iteratively samples from an evolving proposal and reweights both past and new particles via the adaptive multiple importance sampling algorithm until convergence or an early-stop criterion is met; further algorithmic details, theoretical justification, and benchmarks are given in Aalstad et al. (2026).

Table 1. Values of model parameters used in the prior distributions.

Parameter	Unit	Median	Range	Transformed standard deviation
f_{snow}	m w.e. d^{-1} K^{-1}	0.0041	0–0.02	0.4
k_{p}	–	2.17	0–6	0.6
T_{bias}	K	0.021	–10–10	0.25
τ_y	100 kPa	1.453	0–4	0.6

Algorithmically, the AdaPBS is initialized by setting the iteration counter $\ell = 1$ and the initial sampling proposal as the prior $q^{(1)}(\boldsymbol{\theta}) = p(\boldsymbol{\theta})$. The AdaPBS algorithm then proceeds as follows:

1. Sample an ensemble of particles from the current sampling proposal

$$\boldsymbol{\theta}_i^{(\ell)} \sim q^{\boldsymbol{\ell}}(\boldsymbol{\theta}) \tag{5}$$

where $i = 1, \ldots, N_e$ indexes particles in the current ensemble with size N_e.

2. For the entire current particle history, so for all $k = 1, \ldots, \ell$ currently available iterations, and the ensembles of N_e particles from each of these iterations, evaluate the deterministic mixture proposal (Owen and Zhou, 2000)

$$\upsilon(\boldsymbol{\theta}_i^{(k)}) = \frac{1}{\ell} \sum_{j=1}^{\ell} q^{(j)}(\boldsymbol{\theta}_i^{(k)}) \,. \tag{6}$$

3. Compute unnormalized importance weights for all $N_h^{(\ell)} = \ell N_e$ historical particles $\boldsymbol{\theta}_i^{(k)}$ by evaluating the likelihood, prior, and mixture proposal for $k = 1, \ldots, \ell$ and $i = 1 \ldots, N_e$

$$\widetilde{w}_i^{(k)} = \frac{p(\mathbf{y}|\boldsymbol{\theta}_i^{(k)}) p(\boldsymbol{\theta}_i^{(k)})}{\upsilon^{(\ell)}(\boldsymbol{\theta}_i^{(k)})} \,, \tag{7}$$

where, adopting the typical assumption of additive Gaussian observation error $\boldsymbol{\epsilon} \sim \mathcal{N}(\mathbf{0}, \mathbf{R})$ with observation error covariance matrix $\mathbf{R}$ (Alonso-González et al., 2022), the likelihood is given by

$$p(\mathbf{y}|\boldsymbol{\theta}_i^{(k)}) = \det(2\pi\mathbf{R})^{-1/2} \exp\left(-\frac{1}{2} \left[\mathbf{y} - \widehat{\mathbf{y}}_i^{(k)} \right]^{\mathrm{T}} \mathbf{R}^{-1} \left[\mathbf{y} - \widehat{\mathbf{y}}_i^{(k)} \right] \right) , \tag{8}$$

https://doi.org/10.5194/egusphere-2026-1081
Preprint. Discussion started: 4 May 2026

in which $\widehat{\mathbf{y}}_i^{(k)} = \mathcal{G}(\boldsymbol{\theta}_i^{(k)})$ are the modeled observables. Evaluating the likelihood (8) is by far the most expensive step in AdaPBS (and data assimilation in general) since it requires running $\mathcal{G}$, but note that in practice we reuse previous likelihood evaluations from past $k < \ell$ iterations and only need to perform new evaluations for the current iteration $k = \ell$.

4. Compute the normalized weights

$$w_i^k = \frac{\widetilde{w}_i^{(k)}}{\sum_{j=1}^{\ell}\sum_{i=1}^{N_e}\widetilde{w}_i^{(j)}}\,, \tag{9}$$

and the resulting effective sample size (Elvira et al., 2022)

$$N_{\text{eff}}^{(\ell)} = \frac{1}{\sum_{j=1}^{\ell}\sum_{i=1}^{N_e}\left(w_i^k\right)^2}\,, \tag{10}$$

which is a heuristic measure of the diversity of the particle ensemble, where higher values $\gg 1$ are preferable and indicate a diverse ensemble, while lower values $\simeq 1$ are a symptom of degeneracy (ensemble collapse). If $N_{\text{eff}}^{(\ell)} \geq \kappa N_e$ where $0 < \kappa \leq 1$ is the desired diversity threshold, then AdaPBS has converged. If AdaPBS has converged or reached the maximum number of iterations $\ell_{\max}$ (in which case the run is considered unconverged), then this is the final iteration and we set $\ell_{\text{final}} = \ell$. If this is not the final iteration, the clipping procedure of Koblents and Míguez (2015) is applied to improve particle diversity by setting the $\mathcal{T}$ highest non-zero unnormalized weights $\widetilde{w}_i^{(k)}$ equal to the $\mathcal{T}$-th highest unnormalized weight and apply (9) again to obtain clipped normalized weights.

5. Resample (see Chopin and Papaspiliopoulos, 2020) an ensemble of $r = 1, \ldots, N_e$ equally weighted particles $\boldsymbol{\theta}_r^{(\ell)}$ using the (possibly clipped) $N_h^{(\ell)}$ weights $w_i^{(k)}$ from (7) &(9). The index r marks that this is an ensemble of resampled particles, typically including copies, which approximates the posterior as opposed to draws directly from proposals.

6. If this is not the final iteration, define a Gaussian sampling proposal for the next iteration $q^{(\ell+1)}(\boldsymbol{\theta}) = \mathcal{N}(\boldsymbol{\theta}|\boldsymbol{\mu}^{(\ell)}, \mathbf{C}^{(\ell)})$ using the ensemble mean $\boldsymbol{\mu}^{(\ell)}$ and ensemble covariance matrix $\mathbf{C}^{(\ell)}$ from the resampled ensemble $\boldsymbol{\theta}_r^{(\ell)}$ as described in Aalstad et al. (2026). Then set $\ell \leftarrow \ell + 1$ and return to step 1. If this is the final iteration ($\ell_{\text{final}} = \ell$), return the ensemble of N_e equally weighted resampled particles $\boldsymbol{\theta}_r^{(\ell)}$ (and their states) as the posterior ensemble from AdaPBS.

In this study, based on sensitivity experiments and previous work (Aalstad et al., 2026), we set the AdaPBS algorithm parameters as follows: ensemble size $N_e = 200$, maximum number of iterations $\ell_{\max} = 10$, number of particles to clip $\mathcal{T} = 20$, desired diversity threshold $\kappa = 0.1$.

3 Model application and datasets

The hybrid model was tested on 71 marine-terminating glaciers (Table S1) across Svalbard (area range: 3–1,226 km^2; representing approximately 40% of Svalbard's glacier area) that have continuous, complete annual centreline terminus-position records for 2000–2019 (Li et al., 2024), enabling reliable calibration and validation while minimizing artifacts from temporal

https://doi.org/10.5194/egusphere-2026-1081
Preprint. Discussion started: 4 May 2026

gaps. For each glacier, we utilized OGGM to extract the surface elevation, glacier area and width for all 10 m elevation bins according to the Randolph Glacier Inventory (RGIv6) (RGI Consortium, 2017) and digital elevation models. The initial ice thickness for each elevation bin was determined through a mass conserving inversion implemented in OGGM as described by Recinos et al. (2019, 2021), which was constrained by the RGIv6 outlines and elevation data, while also accounting for frontal ablation.

The model was forced with monthly temperature and precipitation from ERA5 (Hersbach et al., 2020). Historical simulations cover 2000–2019, with 2000–2009 used for calibration and 2010–2019 for validation. We produce one model realization for each particle (joint parameters) from the calibrated parameter ensemble, facilitating the evaluation of model performance and uncertainty. For each glacier the model was calibrated and evaluated against: (1) 10-year averaged glacier-wide mass-balance observations for 2000–2009 and 2010–2019 (Hugonnet et al., 2021); and (2) annual time series terminus-position change derived using the methods of Li et al. (2024). Because PyGEM here estimates only the climatic mass balance, we subtracted the frontal-ablation component reported by Kochtitzky et al. (2022) from the mass-balance data of Hugonnet et al. (2021) prior to calibration. We also evaluated the model against 10-year averaged frontal-ablation estimates (2010–2019) obtained via a flux-gate approach (Kochtitzky et al., 2022). Projections for 2000–2100 were forced by an ensemble of 12 general circulation models (GCMs) under two Shared Socioeconomic Pathways, SSP1-2.6 and SSP5-8.5 (SSP126 and SSP585) from the CMIP6 archive for projections (Eyring et al., 2016); see Table S4 for scenario details. For each glacier and scenario we computed ensemble-weighted averages. Future simulation outputs were automatically screened for physical plausibility. We defined a "simulation physical inconsistency" as any case where the projected frontal ablation exceeded the glacier's total mass at that time step. Simulations meeting this criterion—including runs that produced infinite values for specific years, GCMs, or scenarios—were flagged, set to NaN (Not a Number), and the model proceeded with the remaining scenarios. In total, 25 simulations (1.5% of the 1,704 simulations) associated with 3 glaciers were flagged. In addition, one glacier with only a single validated parameter set failed to converge and did not provide a sufficiently large ensemble to quantify future simulation uncertainty. Consequently, we excluded these 4 glaciers from the future projection analyses (Table S1).

4 Hindcast

To aid interpretation of model outputs and workflow, we first present an illustrative hindcast for a single glacier (Sabinebreen) that demonstrates typical model outputs and temporal behavior. This example is provided for methodological clarity and is followed by a quantitative evaluation of hindcast performance across an ensemble of 71 glaciers.

4.1 Illustrative hindcast: Sabinebreen

We present a hindcast for Sabinebreen ($\sim 67\ \mathrm{km}^2$, located on Nordaustlandet in northern Svalbard) as an illustrative case because it benefits from relatively direct, high-quality observations (continuous and dense terminus position time series and velocity measurements) that require minimal interpolation. This makes Sabinebreen a convenient example for demonstrating typical model outputs without artifacts introduced by heavy data infilling. Modeled and observed annual time series of length

https://doi.org/10.5194/egusphere-2026-1081
Preprint. Discussion started: 4 May 2026

change rate and terminus velocity are shown in Figure 1; the hindcast captures both the timing and magnitude of the observed annual terminus changes and reproduces the broad behaviour of terminus velocity.

Although calibration targets are predominantly annual, the model produces monthly estimates of length change and frontal ablation (Figure 2). This higher temporal resolution results from monthly forcings and updates to climatic mass balance and glacier geometry, combined with SERMeQ's ability to resolve monthly terminus-position changes. The Sabinebreen hindcast reveals a pronounced seasonal cycle: retreat typically begins in June, peaks in July–August, and a net advance occurs from September through May. These intra-annual dynamics illustrate the model's ability to represent seasonal behaviour that is not directly constrained by annual calibration data; however, the seasonal amplitude and phasing should be interpreted with caution, as they can be sensitive to the temporal structure of the forcings and to model assumptions about seasonal flow and frontal ablation.

https://doi.org/10.5194/egusphere-2026-1081
Preprint. Discussion started: 4 May 2026

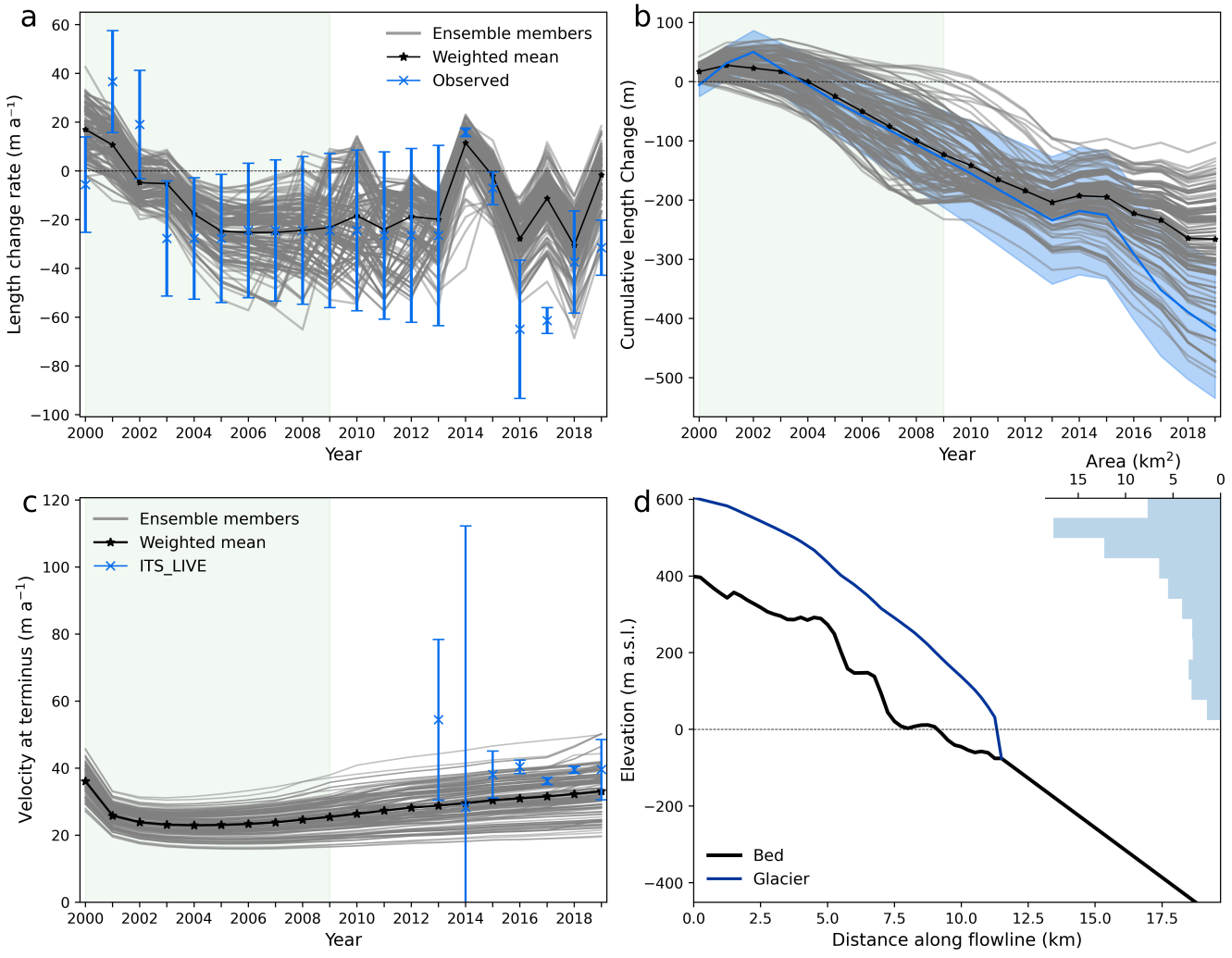

Figure 1. Comparison of modeled results with observations for (a) annual length change rate, (b) cumulative length change, and (c) annual terminus surface velocity of Sabinebreen from 2000 to 2019. Panel (d) shows the initial glacier bed and surface elevation as well as the area-altitude distribution at the year 2000. The observed values in blue include the associated uncertainties. The light green shading refers to the calibration period.

https://doi.org/10.5194/egusphere-2026-1081
Preprint. Discussion started: 4 May 2026

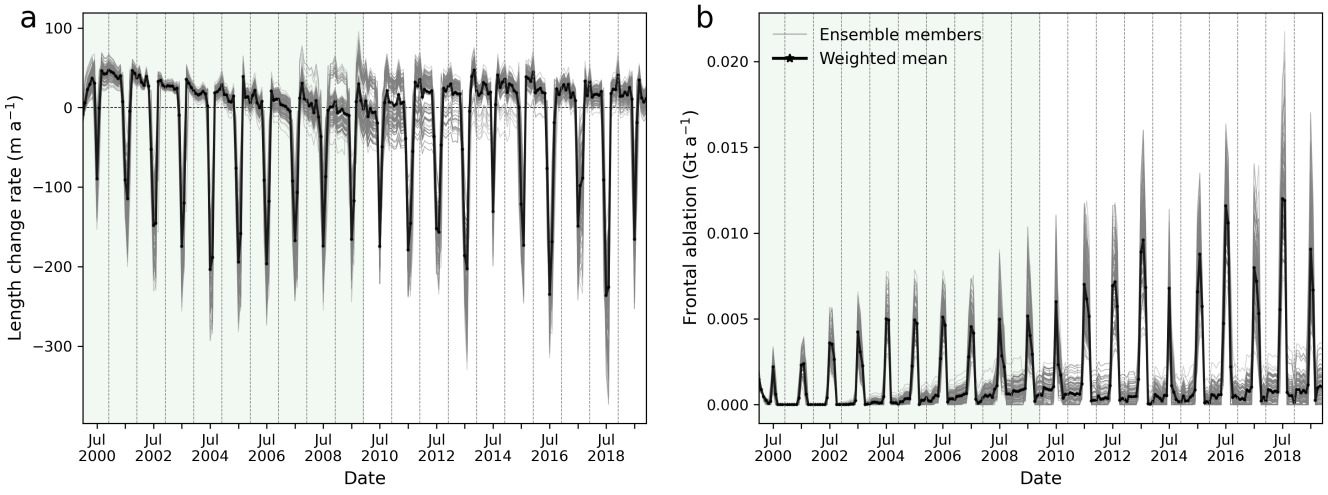

Figure 2. Monthly time series of modeled (a) terminus length changes along the centerline and (b) frontal ablation of Sabinebreen from 2000 to 2019.

4.2 Regional application

Model performance was evaluated via time-split validation across all glaciers for both calibration and validation periods, at glacier and regional scales. The particle-based data assimilation converged to the desired ensemble diversity for 62 glaciers; runs for 9 glaciers did not meet the criterion and terminated at the maximum number of iterations (hereafter referred to as unconverged glaciers). Details of the evaluation procedures and the quantitative metrics are provided in Supplementary Section S2.

At the glacier scale for the 62 converged glaciers during the validation period, the modeled ensemble intervals (2.5 to 97.5%) for total length change and 10-year averaged climatic mass balance generally intersect the 1:1 line (Figure 3 a and c), indicating that modeled central tendencies are broadly consistent with observations despite substantial glacier-to-glacier variability. Many frontal ablation ensembles, however, lie above the 1:1 line (Figure 3e), reflecting a tendency of the model to overestimate frontal ablation for several glaciers. The median normalized continuous ranked probability scores (nCRPS) are 3.2, 1.9 and 4.4 for the three variables, respectively, and the corresponding mean fractional overlaps between the ensemble range (2.5–97.5%) and the observational $\pm 1\sigma$ intervals are 40%, 39% and 34% (Table S2). For context, calibration period results (Figure S1 and Table S2) show lower median nCRPS values and fractional overlaps of similar magnitude compared to the validation period, indicating closer glacier-scale agreement during model fitting.

At the regional scale, modeled and observed cumulative distribution functions (CDF) align closely for all three variables (Figure 3 b, d, f and S1b, d, f), with an overall CDF overlap $\geq$95% (Table S2). It indicates strong agreement in the aggregated distributions during both periods despite the remaining per-glacier mismatches. Across both periods, the 9 unconverged glaciers consistently show weaker performance (Figures 3 and S1, and Table S3).

https://doi.org/10.5194/egusphere-2026-1081
Preprint. Discussion started: 4 May 2026

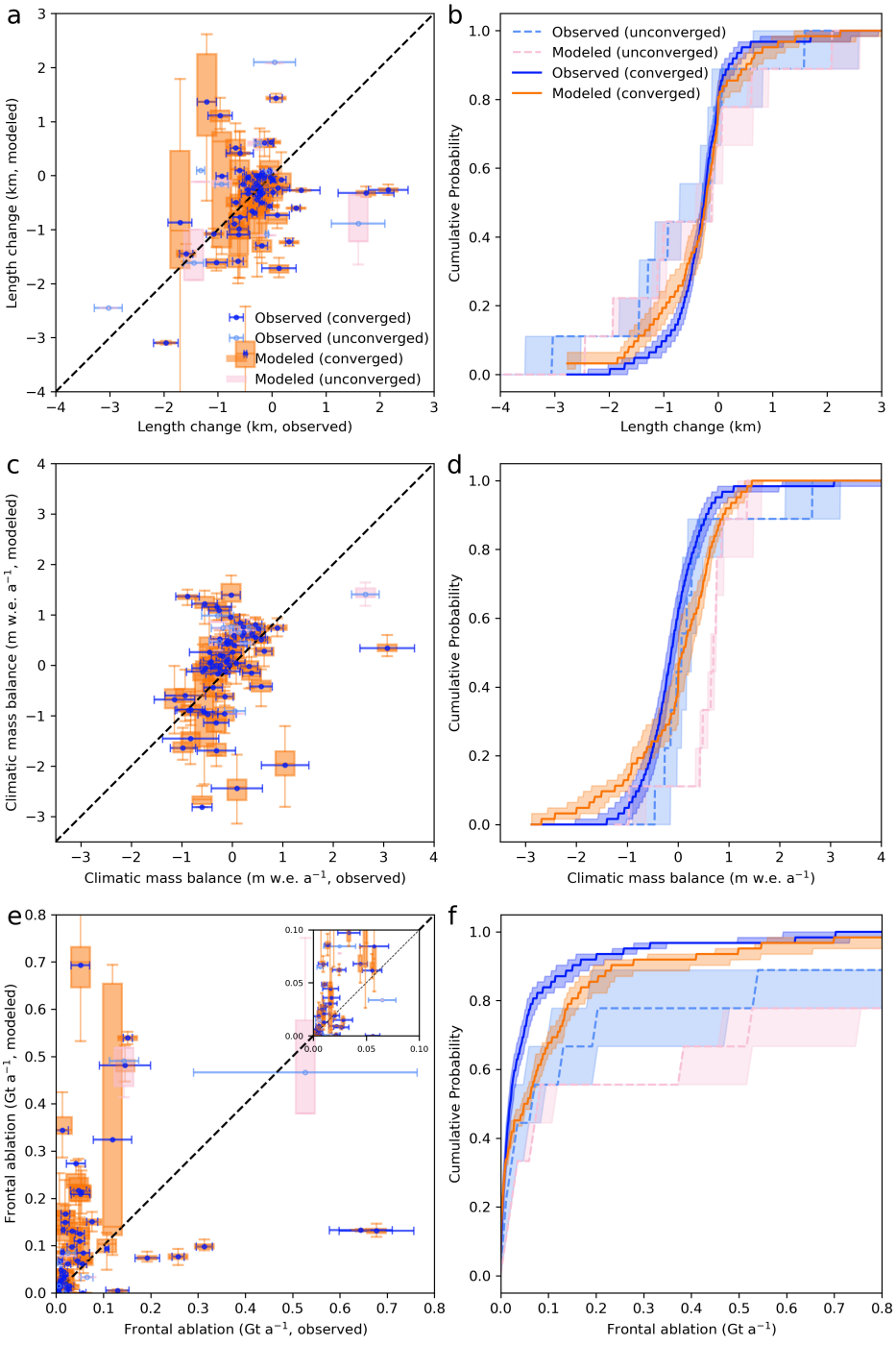

Figure 3. Validation of modeled results against observations for 71 glaciers in Svalbard from 2010 to 2019. (**a, b**) Total length change along the glacier centerline; (**c, d**) Mean climatic mass balance; (**e, f**) Mean frontal ablation. Panels (**a, c, e**) show observations (blue error bar) and modeled ensemble means (orange box represents the interquartile range (IQR) of the ensemble of each glacier). Panels (**b, d, f**) illustrates the empirical cumulative distribution functions (CDFs) for observations (blue line ± 95% confidence interval via Monte Carlo sampling) and model results (orange line ± ensemble range).

https://doi.org/10.5194/egusphere-2026-1081
Preprint. Discussion started: 4 May 2026

5 Projections

The projected cumulative glacier length changes throughout the 21st century for SSP126 and SSP585 are presented as the multi-GCM median, accompanied by the interquartile range (IQR) in Figure 4. By 2100, the median projected length change for most individual glaciers under both scenarios lies between -5 km and 5 km. The majority of glaciers are expected to retreat, while only a few show changes close to zero and some exhibit clear advances. In particular, projected length change differed in sign (advance versus retreat or vice versa) between the two scenarios for eight glaciers, most of which are identified as surging in the RGIv6 dataset. The mean difference in glacier length change between the two scenarios is modest compared with the associated uncertainty, with SSP585 producing about 0.9 km (0.9%) more retreat than SSP126 on average across all glaciers. There is no clear systematic difference between the scenarios for individual glaciers, suggesting that glacier length changes may be largely insensitive to the choice of climatic forcing scenario.

At the regional scale, mass change differs substantially between the two scenarios, particularly after 2050. The cumulative components of glacier mass change—frontal ablation and climatic mass balance—for all 67 glaciers over 2000–2100 are shown in Figure 5. The mean rate of increase in cumulative frontal ablation is higher under SSP585 than under SSP126 over the full period (9.0 Gt a^{-1} vs. 7.0 Gt a^{-1}), and this contrast strengthens after 2050 (9.6 Gt a^{-1} vs. 6.3 Gt a^{-1} for 2050–2100). Under SSP126, cumulative climatic mass balance increases at a mean rate of 5.9 Gt a^{-1} over 2000–2100. In contrast, SSP585 is characterized by a positive rate of cumulative climatic mass balance before 2050 (5.8 Gt a^{-1}), but a negative rate thereafter, reaching -9.0 Gt a^{-1} after 2080, coincident with intensified frontal ablation (7.8 Gt a^{-1}). Uncertainties are small before 2030 but increase markedly thereafter, particularly for climatic mass balance, and are consistently larger under SSP585 than under SSP126.

https://doi.org/10.5194/egusphere-2026-1081
Preprint. Discussion started: 4 May 2026

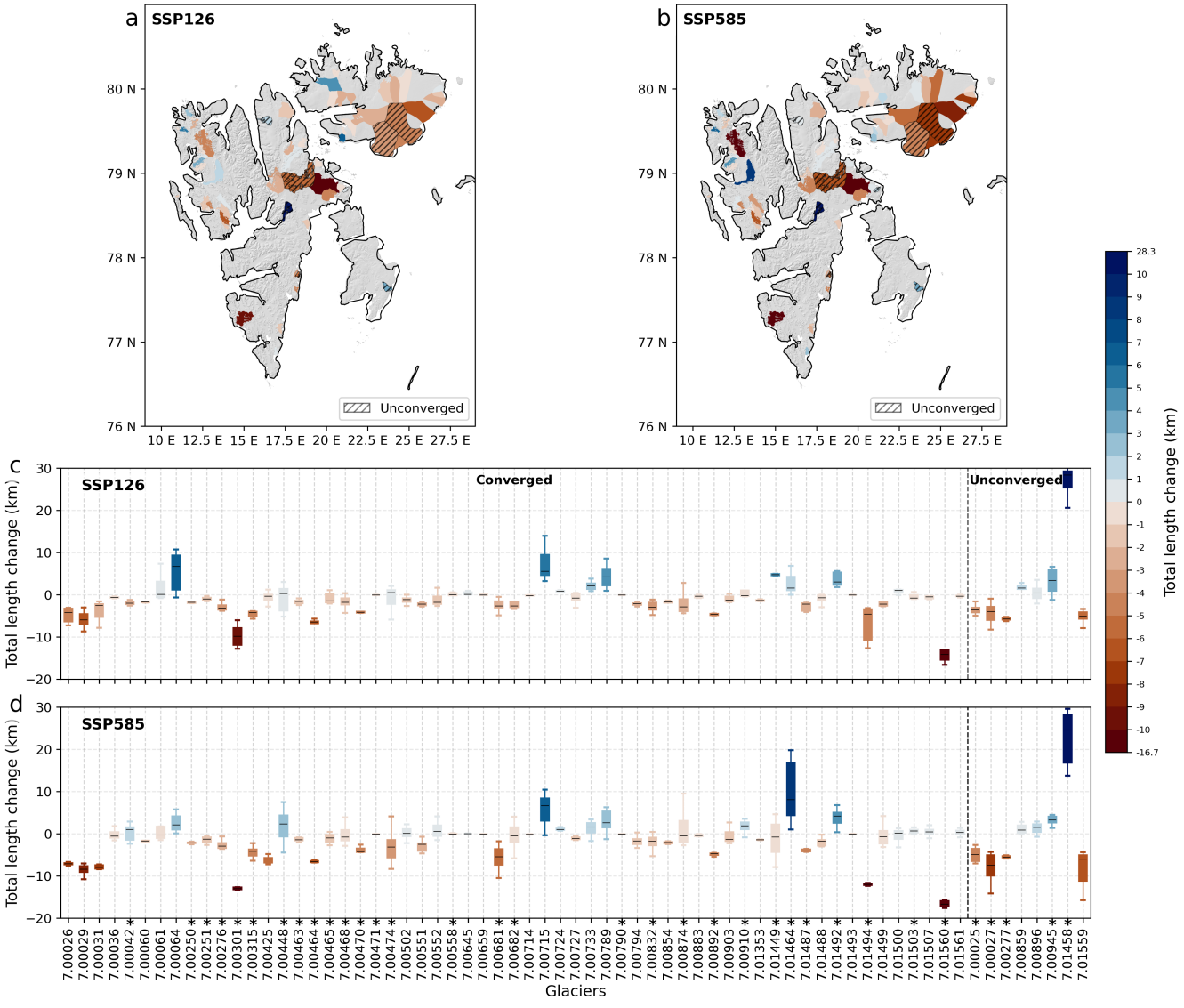

Figure 4. Projected total length changes at the terminus along the centerlines for 67 glaciers in Svalbard from 2000 to 2100. (**a-b**) Spatial distribution of median length changes under SSP126 and SSP585 scenarios, with hashed areas indicating unconverged calibrations (9 glaciers). (**c, d**) Distribution of projected total length change of each glacier under scenarios SSP126 and SSP585, grouped by glaciers with converged calibrations (left) and unconverged (right). Box elements: the center line indicates the median, the box spans the 25th–75th percentiles (interquartile ranges, IQR), and the whiskers extend to 1.5×IQR. Color scale represents magnitude of length change, facilitating comparison between spatial and statistical representations. Glaciers are identified by their RGIv6 IDs listed without the common "RGI60-0" prefix, and surge-type glaciers are marked with an asterisk (*).

https://doi.org/10.5194/egusphere-2026-1081
Preprint. Discussion started: 4 May 2026

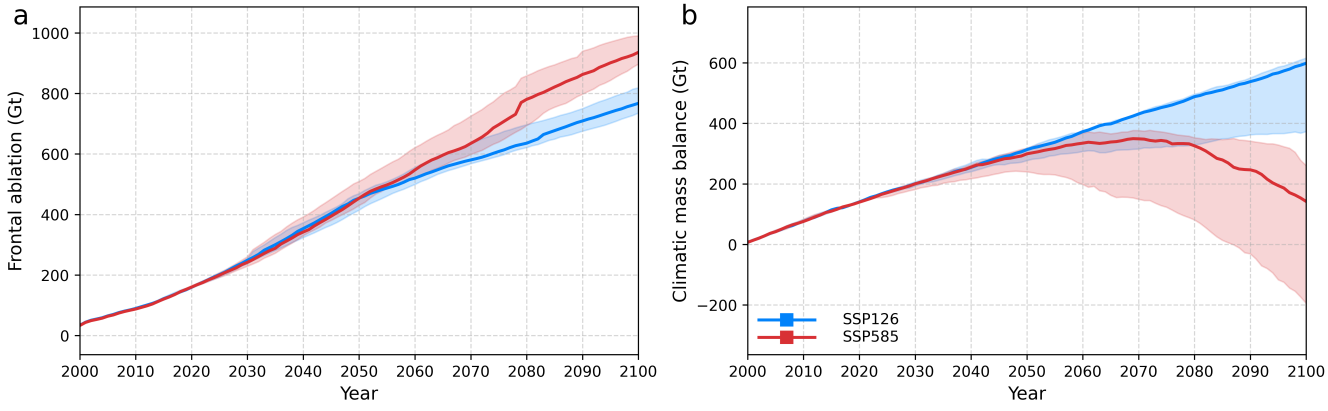

Figure 5. Projected cumulative mass change from 2000–2100 for 67 glaciers for two SSPs and 12 GCMs. (**a**) Frontal ablation; (**b**) Climatic mass balance. Solid lines and shaded areas depict median values and interquartile ranges (25th–75th percentiles, IQR), respectively.

6 Discussion

6.1 Calibration Strategy and Model Performance

To overcome the limitations and circularity of previous disjoint component-wise calibration strategies, we implement a joint calibration framework using the AdaPBS method, which simultaneously infers all parameters in the coupled model. As in previous implementations, we assume these parameters are time-invariant in the current setup. This joint approach inherently improves consistency and reduces cross-component bias. A key step in making joint calibration possible was the use of the AdaPBS algorithm (Aalstad et al., 2026), making inference more stable than PBS (Margulis et al., 2015) and faster than MCMC (Rounce et al., 2020b) while ensuring efficiency by recycling historical particles used at each iteration.

Effective implementation of AdaPBS depends on careful tuning of its hyperparameters (that is, the algorithm parameter settings), because these choices directly affect both the model's performance and the required computational resources. After initially exploring and manually testing various hyperparameter configurations on a handful of glaciers, we selected a particle count of $N_e = 200$, an effective sample size-based diversity threshold of $\kappa = 0.1$, and a maximum of $\ell_{\max} = 10$ iterations. This combination provides a favorable trade-off between efficiency and accuracy at the regional scale. However, the method remains inherently sensitive to the choice of diversity threshold and maximum number of iterations. It is thus likely that our results could be improved further by more judicious tuning of hyperparameters, especially the maximum number of iterations. For challenging individual glaciers that still require more robust convergence, these hyperparameters could be manually adjusted for the specific glacier in question by increasing the maximum number of iterations after the fact. Hyperparameter tuning could also be automated through the use of Bayesian optimization (Garnett, 2023). Nonetheless, rigorous hyperparameter tuning remains beyond the scope of this work, which focuses on presenting a new hybrid global glacier modeling and calibration

https://doi.org/10.5194/egusphere-2026-1081
Preprint. Discussion started: 4 May 2026

framework. The AdaPBS method improved the posterior compared with the prior for both converged and unconverged cases (See details in Supplement Section S3 and Figure S2).

We also note that within our coupling framework, SERMeQ outputs the terminus position change explicitly along the flowline at each time step, whereas OGGM updates the glacier profile using elevation-band flowlines. Figure S3 highlights the importance of resolving terminus changes along the flowline. On very flat glaciers, individual elevation bands span uneven horizontal distances (the length of each band along the flowline depends on the local slope), which limits the ability of an elevation-band representation to capture small but important terminus displacements.

Despite these strengths, an important glacier-scale limitation remains: the systematic overestimation of frontal ablation, which highlights shortcomings in how terminus dynamics are represented and constrained. This bias may arise from compounded uncertainties in the initial flowline geometry (e.g., bed, thickness, and width), errors in derived velocities, and the fact that velocity is only indirectly constrained by observations. Together, these issues point to the need for more accurate bed inversions and better-constrained velocity estimates to improve glacier-scale frontal ablation estimates.

6.2 Physical Instabilities and Model Limitations

Frontal ablation exhibits episodic behavior, thereby increasing the probability of dynamic instabilities at the terminus (Kochtitzky et al., 2023; Benn et al., 2017; Luckman et al., 2015). This phenomenon is exemplified by observations in Svalbard, where instances of "simulation physical inconsistency" are noted above. In our future projection simulations, as a result of these physical failures, we excluded three glaciers from our future simulation. Among the three glaciers (two converged simulations and one unconverged), potential explanations include anomalous or extreme climate forcing from certain GCMs; errors or inconsistencies in the initial glacier geometry (e.g., surface elevation, ice thickness, or total mass) and the modeled velocity; and limitations of, or extrapolations in, the model formulation and parameterizations under the projected climate conditions (Marzeion et al., 2020; Schuster et al., 2023). These physical inconsistencies underscore the sensitivity of projections to input quality and parameter bounds. Where possible, we inspected raw forcing time series and initialization files to identify physical inconsistency; however, fully resolving these cases will require additional work — such as more rigorous bias correction, recalibration for out-of-range conditions, or incorporation of missing physical processes — to reduce the associated uncertainties in the ensemble projections.

Additionally, one glacier was removed from the projection analysis because the AdaPBS algorithm remained far from convergence, with complete ensemble collapse manifested by only a single surviving parameter vector ($N_{\text{eff}} = 1$) even after the maximum number of $\ell_{\max} = 10$ and 100 iterations. The large observational noise for this glacier appears to be one obstacle to achieving calibration convergence. It is important to emphasize that the results presented in this study are obtained under a fixed hyperparameters setting and should be viewed as an illustration of the method's application to these glaciers, rather than as a definitive or fully optimized solution.

https://doi.org/10.5194/egusphere-2026-1081
Preprint. Discussion started: 4 May 2026

6.3 Surge-Type Glaciers: A Special Case?

A high proportion of Svalbard's marine-terminating glaciers surge. Glacier surges are typically viewed as internal instabilities (Meier and Post, 1969), characterized by cyclical flow between extended quiescent periods and brief surge events. The occurrence of surges is largely unpredictable and is not thought to be driven directly by external factors (Bhambri et al., 2017; Sharp, 1988). Thirty-six out of 71 glaciers in our study were classified as surge-type by the RGIv6 (RGI Consortium, 2017). Notably, our model did not include any specific design features for surge-type glaciers, and we did not observe any significant differences in the calibration, simulation, or future projection processes when compared to non-surge glaciers. Exceptions were limited to a subset of glaciers exhibiting pronounced disparities in length change between scenarios; for example, those that advanced under SSP126 but retreated under SSP585, or vice versa, with the majority of these cases involving surge-type glaciers. This highlights the challenges surge-type glaciers pose for standard modeling approaches and emphasizes the need for tailored treatment in future model refinements.

Besides, many surge events are episodic and lack long-term documentation. Our frontal ablation model, grounded in seasonal to annual-averaged stress fields that do not account for subglacial hydrology, was not specifically designed for surge-type glaciers. Consequently, it should not be expected to capture the extreme terminus dynamics during surges. Our simulations showed limited influence of surge type over the calibration and validation period, but future projections should be interpreted with the caveat that un-simulated surge cycles may dramatically alter front positions for short periods.

7 Conclusion

This study demonstrates that the coupled model effectively reproduces observed glacier length changes and mass balance trends of marine-terminating glaciers across Svalbard from 2000 to 2019, particularly for glaciers where convergence was achieved. The model successfully generated monthly estimates of both length changes and mass balance components, and the joint calibration method proved efficient for parameter estimation and uncertainty quantification. While total length changes and climatic mass balance are generally well represented at both regional and glacier scales, frontal ablation tends to be overestimated at the glacier scale. Despite this limitation, the model is well suited for capturing glacier change in an aggregated, regional sense and provides a robust framework for projecting future glacier dynamics under different climate scenarios.

Overall, the results underscore the model's capability to reproduce seasonal variations of marine-terminating glaciers and to project future glacier evolution, offering valuable insights into regional contributions to sea-level rise and freshwater availability. The framework is extendable to lake-terminating glaciers and, more broadly, to a global scale for marine-terminating glaciers. Future improvements may include using more advanced dynamic models (e.g., 2D or 3D), refining initial geometries to more accurately represent ice thickness, and implementing specialized treatments for surge-type and floating-terminus glaciers to improve predictive skill. Collectively, these developments would constitute a step-change in our ability to predict the behavior of marine-terminating glaciers.

https://doi.org/10.5194/egusphere-2026-1081
Preprint. Discussion started: 4 May 2026

Code and data availability. The code for the coupling model framework is available through zenodo https://doi.org/10.5281/zenodo.18761730 (Yang and Debolskiy, 2026); which is based on OGGM v1.6.2 https://doi.org/10.5281/zenodo.13371106 (Maussion et al., 2024), and PyGEM v0.2.0 https://doi.org/10.5281/zenodo.15045308 (Rounce, 2022), and SERMeQ v1.0.0 https://doi.org/10.5281/zenodo.4075607 (Ultee, 2020). Calibration datasets for Svalbard, including mass balance data available at Hugonnet et al. (2021), frontal ablation data at Kochtitzky et al. (2022), and frontal change data at Li et al. (2024). The model output are available at https://doi.org/10.11582/2026.7whvas95 Yang (2026).

Author contributions. RY and LU designed the coupling structure. RY implemented the SERMeQ-PyGEM-OGGM coupling using open-source SERMeQ, OGGM and PyGEM code, with guidance from PS. KA and RY developed all calibration methods. RY and MD structured the code, while RY conducted all analyses and created all figures. RY, LU, and KA drafted the manuscript. RH conceived the project and secured funding. TL calculated the annual time series front change data of glacier in Svalbard from 2000 to 2019. DR provided support with PyGEM. RY, LU, KA, RH and DR discussed the content and provided text reviews and edits on the manuscript.All co-authors have read and approved the manuscript.

Competing interests. The authors declare no conflicts of interest relevant to this study.

Acknowledgements. This work is supported by ERC-2022-ADG under Grant 101096057 GLACMASS and NRC Project 324131. The simulations were performed on resources (under NN11115K/ NS11115K) provided by Sigma2 - the National Infrastructure for High-Performance Computing and Data Storage in Norway. We thank Fabien Maussion (University of Bristol) for valuable comments and suggestions.

https://doi.org/10.5194/egusphere-2026-1081
Preprint. Discussion started: 4 May 2026

References

Aalstad, K., Alonso-González, E., Pirk, N., Westermann, S., Willmes, C., and Yang, R.: Evolving beyond collapse: An adaptive particle batch smoother for cryospheric data assimilation, arXiv, https://doi.org/10.48550/arXiv.2601.20049, preprint, 2026.

Alonso-González, E., Aalstad, K., Baba, M. W., Revuelto, J., López-Moreno, J. I., Fiddes, J., Essery, R., and Gascoin, S.: The Multiple Snow Data Assimilation System (MuSA v1.0), Geosci. Model Dev., https://doi.org/10.5194/gmd-15-9127-2022, 2022.

Bassis, J. N. and Ultee, L.: A thin film viscoplastic theory for calving glaciers: Towards a bound on the calving rate of glaciers, Journal of Geophysical Research: Earth Surface, 124, https://doi.org/10.1029/2019JF005160, 2019.

Benn, D. I., Warren, C. R., and Mottram, R. H.: Calving processes and the dynamics of calving glaciers, Earth-Science Reviews, 82, 143–179, https://doi.org/10.1016/j.earscirev.2007.02.002, 2007.

Benn, D. I., Cowton, T., Todd, J., and Luckman, A.: Glacier Calving in Greenland, Curr Clim Change Rep, 3, 282–290, https://doi.org/10.1007/s40641-017-0070-1, 2017.

Bhambri, R., Hewitt, K., Kawishwar, P., and Pratap, B.: Surge-Type and Surge-Modified Glaciers in the Karakoram, 7, 15 391, https://doi.org/10.1038/s41598-017-15473-8, 2017.

Brown, C. S.: Calving Speed of Alaska Tidewater Glaciers, with Application to Columbia Glacier, no. 1258 in Geological Survey Professional Paper, U.S. Dept. of the Interior, Geological Survey ; For sale by the Distribution Branch, U.S. Geological Survey, Reston, Va.?] : Alexandria, Va., 1983.

Bugallo, M. F., Elvira, V., Martino, L., Luengo, D., Miguez, J., and Djuric, P. M.: Adaptive Importance Sampling: The past, the present, and the future, IEEE Signal Processing Magazine, 34, 60–79, https://doi.org/10.1109/MSP.2017.2699226, 2017.

Cao, W., Aalstad, K., Schmidt, L., Westermann, S., and Schuler, T.: Bayesian data assimilation on an Arctic glacier: Learning from large ensemble twin experiments, Journal of Glaciology, pp. 1–44, https://doi.org/10.1017/jog.2025.10101, 2025.

Chopin, N. and Papaspiliopoulos, O.: An Introduction to Sequential Monte Carlo, Springer, https://doi.org/10.1007/978-3-030-47845-2, 2020.

Cogley, J. G., Hock, R., Rasmussen, L. A., Arendt, A. A., Bauder, A., Braithwaite, R. J., Jansson, P., Kaser, G., Möller, M., Nicholson, L., and Zemp, M.: Glossary of Glacier Mass Balance and Related Terms, IHP-VII Technical Documents in Hydrology No. 86, IACS Contribution No. 2, UNESCO-IHP, Paris., 2011.

Cornuet, J.-M., Marin, J.-M., Antonietta, M., and Robert, C.: Adaptive Multiple Importance Sampling, Scandinavian Journal of Statistics, 39, 798–812, https://doi.org/10.1111/j.1467-9469.2011.00756.x, 2012.

Cuffey, K. M. and Paterson, W. S. B.: The Physics of Glaciers, Academic Press, ISBN 0-08-091912-X, 2010.

Elvira, V., Martino, L., and Robert, C.: Rethinking the Effective Sample Size, International Statistical Review, 90, 525–550, https://doi.org/10.1111/insr.12500, 2022.

Evensen, G., Vossepoel, F. C., and van Leeuwen, P. J.: Data Assimilation Fundamentals, Springer, https://doi.org/10.1007/978-3-030-96709-3, 2022.

Eyring, V., Bony, S., Meehl, G. A., Senior, C. A., Stevens, B., Stouffer, R. J., and Taylor, K. E.: Overview of the Coupled Model Intercomparison Project Phase 6 (CMIP6) Experimental Design and Organization, 9, 1937–1958, https://doi.org/10.5194/gmd-9-1937-2016, 2016.

https://doi.org/10.5194/egusphere-2026-1081
Preprint. Discussion started: 4 May 2026

Gardner, A. S., Moholdt, G., Cogley, J. G., Wouters, B., Arendt, A. A., Wahr, J., Berthier, E., Hock, R., Pfeffer, W. T., Kaser, G., Ligtenberg, S. R. M., Bolch, T., Sharp, M. J., Hagen, J. O., van den Broeke, M. R., and Paul, F.: A Reconciled Estimate of Glacier Contributions to Sea Level Rise: 2003 to 2009, science, 340, 852–857, https://doi.org/10.1126/science.1234532, 2013.

Garnett, R.: Bayesian Optimization, Cambridge University Press, https://doi.org/10.1017/9781108348973, 2023.

Hanson, B. and Hooke, R. L.: Glacier calving: a numerical model of forces in the calving-speed/water-depth relation, Journal of Glaciology, 46, 188–196, https://doi.org/10.3189/172756500781832792, 2000.

Hersbach, H., Bell, B., Berrisford, P., Hirahara, S., Horányi, A., Muñoz-Sabater, J., Nicolas, J., Peubey, C., Radu, R., Schepers, D., Simmons, A., Soci, C., Abdalla, S., Abellan, X., Balsamo, G., Bechtold, P., Biavati, G., Bidlot, J., Bonavita, M., De Chiara, G., Dahlgren, P., Dee, D., Diamantakis, M., Dragani, R., Flemming, J., Forbes, R., Fuentes, M., Geer, A., Haimberger, L., Healy, S., Hogan, R. J., Hólm, E., Janisková, M., Keeley, S., Laloyaux, P., Lopez, P., Lupu, C., Radnoti, G., de Rosnay, P., Rozum, I., Vamborg, F., Villaume, S., and Thépaut, J.-N.: The ERA5 global reanalysis, Quarterly Journal of the Royal Meteorological Society, 146, 1999–2049, https://doi.org/https://doi.org/10.1002/qj.3803, 2020.

Hugonnet, R., McNabb, R., Berthier, E., Menounos, B., Nuth, C., Girod, L., Farinotti, D., Huss, M., Dussaillant, I., Brun, F., and Kääb, A.: Accelerated global glacier mass loss in the early twenty-first century, Nature, 592, 726–731, https://doi.org/10.1038/s41586-021-03436-z, 2021.

Huss, M. and Hock, R.: A New Model for Global Glacier Change and Sea-Level Rise, Frontiers in Earth Science, 3, https://doi.org/10.3389/feart.2015.00054, 2015.

Koblents, E. and Míguez, J.: A population Monte Carlo scheme with transformed weights and its application to stochastic kinetic models, Statistics and Computing, 25, 407–425, https://doi.org/10.1007/s11222-013-9440-2, 2015.

Kochtitzky, W., Copland, L., Van Wychen, W., Hugonnet, R., Hock, R., Dowdeswell, J. A., Benham, T., Strozzi, T., Glazovsky, A., Lavrentiev, I., Rounce, D. R., Millan, R., Cook, A., Dalton, A., Jiskoot, H., Cooley, J., Jania, J., and Navarro, F.: The Unquantified Mass Loss of Northern Hemisphere Marine-Terminating Glaciers from 2000–2020, Nat Commun, 13, 5835, https://doi.org/10.1038/s41467-022-33231-x, 2022.

Kochtitzky, W., Copland, L., Wychen, W. V., Hock, R., Rounce, D. R., Jiskoot, H., Scambos, T. A., Morlighem, M., King, M., Cha, L., Gould, L., Merrill, P.-M., Glazovsky, A., Hugonnet, R., Strozzi, T., Noël, B., Navarro, F., Millan, R., Dowdeswell, J. A., Cook, A., Dalton, A., Khan, S., and Jania, J.: Progress toward Globally Complete Frontal Ablation Estimates of Marine-Terminating Glaciers, Annals of Glaciology, pp. 1–10, https://doi.org/10.1017/aog.2023.35, 2023.

Landmann, J. M., Künsch, H. R., Huss, M., Ogier, C., Kalisch, M., and Farinotti, D.: Assimilating near-real-time mass balance stake readings into a model ensemble using a particle filter, The Cryosphere, 15, 5017–5040, https://doi.org/10.5194/tc-15-5017-2021, 2021.

Li, T., Heidler, K., Mou, L., Ignéczi, Á., Zhu, X. X., and Bamber, J. L.: A High-Resolution Calving Front Data Product for Marine-Terminating Glaciers in Svalbard, Earth System Science Data, 16, 919–939, https://doi.org/10.5194/essd-16-919-2024, 2024.

Luckman, A., Benn, D. I., Cottier, F., Bevan, S., Nilsen, F., and Inall, M.: Calving Rates at Tidewater Glaciers Vary Strongly with Ocean Temperature, Nature communications, 6, 8566, https://doi.org/10.1038/ncomms9566, 2015.

Malles, J.-H., Maussion, F., Ultee, L., Kochtitzky, W., Copland, L., Marzeion, B., Maussion, F., Ultee, L., Kochtitzky, W., Copland, L., and Marzeion, B.: Exploring the Impact of a Frontal Ablation Parameterization on Projected 21st-Century Mass Change for Northern Hemisphere Glaciers, Journal of Glaciology, 69, 1317–1332, https://doi.org/10.1017/jog.2023.19, 2023.

Margulis, S. A., Girotto, M., Cortés, G., and Durand, M.: A Particle Batch Smoother Approach to Snow Water Equivalent Estimation, Journal of Hydrometeorology, https://doi.org/10.1175/JHM-D-14-0177.1, 2015.

https://doi.org/10.5194/egusphere-2026-1081
Preprint. Discussion started: 4 May 2026

Marzeion, B., Jarosch, A. H., and Hofer, M.: Past and future sea-level change from the surface mass balance of glaciers, The Cryosphere, 6, 1295–1322, https://doi.org/10.5194/tc-6-1295-2012, 2012.

Marzeion, B., Hock, R., Anderson, B., Bliss, A., Champollion, N., Fujita, K., Huss, M., Immerzeel, W., Kraaijenbrink, P., Malles, J.-H., Maussion, F., Radić, V., Rounce, D. R., Sakai, A., Shannon, S., van de Wal, R., and Zekollari, H.: Partitioning the Uncertainty of Ensemble Projections of Global Glacier Mass Change, Earth's Future, p. e2019EF001470, https://doi.org/10.1029/2019EF001470, 2020.

Maussion, F., Butenko, A., Champollion, N., Dusch, M., Eis, J., Fourteau, K., Gregor, P., Jarosch, A. H., Landmann, J., Oesterle, F., Recinos, B., Rothenpieler, T., Vlug, A., Wild, C. T., and Marzeion, B.: The Open Global Glacier Model (OGGM) v1.1, Geoscientific Model Development, 12, 909–931, https://doi.org/10.5194/gmd-12-909-2019, 2019.

Maussion, F., Rothenpieler, T., Dusch, M., Schmitt, P., Vlug, A., Schuster, L., Champollion, N., Li, F., Fischer, A., Marzeion, B., Oberrauch, M., Eis, J., Landmann, J., Jarosch, A., luzpaz, Hanus, S., bowenbelongstonature, Minallah, S., Bartholomew, S. L., Castellani, M., Rounce, D., zhaohongyu, shuoer86, rebneugebauer, Gregor, P., omahs, dngoldberg, anton ub, and Thompson, S.: OGGM/oggm: v1.6.2, https://doi.org/10.5281/zenodo.13371106, zenodo [code], 2024.

Meier, M. F. and Post, A.: What are glacier surges?, Canadian Journal of Earth Sciences, https://doi.org/10.1139/e69-081, publisher: NRC Research Press Ottawa, Canada, 1969.

Murphy, K.: Probabilistic Machine Learning: Advanced Topics, MIT Press, http://probml.github.io/book2, 2023.

Muñoz-Hermosilla, J. M., Otero, J., De Andrés, E., Shahateet, K., Navarro, F., and Pérez-Doña, I.: A 3D glacier dynamics–line plume model to estimate the frontal ablation of Hansbreen, Svalbard, The Cryosphere, 18, 1911–1924, https://doi.org/10.5194/tc-18-1911-2024, publisher: Copernicus GmbH, 2024.

Navari, M., Margulis, S. A., Tedesco, M., Fettweis, X., and van de Wal, R. S. W.: Reanalysis Surface Mass Balance of the Greenland Ice Sheet Along K-Transect (2000–2014), Geophysical Research Letters, 48, e2021GL094 602, https://doi.org/https://doi.org/10.1029/2021GL094602, 2021.

Nick, F., van der Veen, C., Vieli, A., and Benn, D.: A physically based calving model applied to marine outlet glaciers and implications for the glacier dynamics, Journal of Glaciology, 56, 781–794, https://doi.org/10.3189/002214310794457344, 2010.

Oerlemans, J. and Nick, F. M.: A minimal model of a tidewater glacier, Annals of Glaciology, 42, 1–6, https://doi.org/10.3189/172756405781813023, 2005.

O'Neel, S., Pfeffer, W. T., Krimmel, R., and Meier, M.: Evolving Force Balance at Columbia Glacier, Alaska, during Its Rapid Retreat, Journal of Geophysical Research: Earth Surface, 110, https://doi.org/10.1029/2005JF000292, 2005.

Otero, J., Navarro, F. J., Martin, C., Cuadrado, M. L., and Corcuera, M. I.: A three-dimensional calving model: numerical experiments on Johnsons Glacier, Livingston Island, Antarctica, Journal of Glaciology, 56, 200–214, https://doi.org/10.3189/002214310791968539, 2010.

Owen, A. and Zhou, Y.: Safe and Effective Importance Sampling, Journal of the American Statistical Association, 95, 135–143, https://doi.org/10.1080/01621459.2000.10473909, 2000.

Pelto, M. S. and Warren, C. R.: Relationship between Tidewater Glacier Calving Velocity and Water Depth at the Calving Front, Ann. Glaciol., 15, 115–118, https://doi.org/10.3189/S0260305500009617, 1991.

Recinos, B., Maussion, F., Rothenpieler, T., and Marzeion, B.: Impact of frontal ablation on the ice thickness estimation of marine-terminating glaciers in Alaska, The Cryosphere, 13, 2657–2672, https://doi.org/https://doi.org/10.5194/tc-13-2657-2019, 2019.

Recinos, B., Maussion, F., Noël, B., Möller, M., and Marzeion, B.: Calibration of a frontal ablation parameterisation applied to Greenland's peripheral calving glaciers, Journal of Glaciology, 67, 1177–1189, https://doi.org/10.1017/jog.2021.63, 2021.

https://doi.org/10.5194/egusphere-2026-1081
Preprint. Discussion started: 4 May 2026

RGI Consortium: Randolph Glacier Inventory – A Dataset of Global Glacier Outlines: Version 6.0, Technical Report, Global Land Ice Measurements from Space, 2017.

Rounce, D.: PyGEMv0.2.0, https://doi.org/10.5281/zenodo.15045308, 2022.

Rounce, D. R., Hock, R., and Shean, D. E.: Glacier Mass Change in High Mountain Asia Through 2100 Using the Open-Source Python Glacier Evolution Model (PyGEM), Frontiers in Earth Science, 7, https://doi.org/10.3389/feart.2019.00331, 2020a.

Rounce, D. R., Khurana, T., Short, M. B., Hock, R., Shean, D. E., and Brinkerhoff, D. J.: Quantifying parameter uncertainty in a large-scale glacier evolution model using Bayesian inference: application to High Mountain Asia, Journal of Glaciology, 66, 175–187, https://doi.org/10.1017/jog.2019.91, 2020b.

Rounce, D. R., Hock, R., Maussion, F., Hugonnet, R., Kochtitzky, W., Huss, M., Berthier, E., Brinkerhoff, D., Compagno, L., Copland, L., Farinotti, D., Menounos, B., and McNabb, R. W.: Global glacier change in the 21st century: Every increase in temperature matters, Science, 379, 78–83, https://doi.org/10.1126/science.abo1324, 2023.

Schuster, L., Rounce, D. R., and Maussion, F.: Glacier projections sensitivity to temperature-index model choices and calibration strategies, Annals of Glaciology, pp. 1–16, https://doi.org/DOI: 10.1017/aog.2023.57, 2023.

Sharp, M.: Surging Glaciers: Behaviour and Mechanisms, 12, 349–370, https://doi.org/10.1177/030913338801200302, 1988.

Sjursen, K. H., Dunse, T., Schuler, T. V., Andreassen, L. M., and Åkesson, H.: Spatiotemporal mass-balance variability of Jostedalsbreen Ice Cap, Norway, revealed by a temperature-index model using Bayesian inference, Annals of Glaciology, 66, e1, https://doi.org/10.1017/aog.2024.41, 2025.

Ultee, L.: ehultee/plastic-networks: Initial release, https://doi.org/10.5281/zenodo.4075607, zenodo [code], 2020.

Ultee, L. and Bassis, J. N.: The future is Nye: An extension of the perfect plastic approximation to tidewater glaciers, Journal of Glaciology, 62, 1143–1152, https://doi.org/10.1017/jog.2016.108, 2016.

Ultee, L. and Bassis, J. N.: SERMeQ Model Produces a Realistic Upper Bound on Calving Retreat for 155 Greenland Outlet Glaciers, Geophysical Research Letters, 47, e2020GL090 213, https://doi.org/10.1029/2020GL090213, 2020.

van der Veen, C. J.: Calving Glaciers, Progress in Physical Geography: Earth and Environment, 26, 96–122, https://doi.org/10.1191/0309133302pp327ra, 2002.

Vieli, A., Funk, M., and Blatter, H.: Flow dynamics of tidewater glaciers: a numerical modelling approach, Journal of Glaciology, 47, 595–606, https://doi.org/10.3189/172756501781831747, 2001.

Willmes, C., Aalstad, K., and Westermann, S.: Assimilating high-resolution satellite snow cover data in a permafrost model, EGUsphere, https://doi.org/10.5194/egusphere-2025-3142, 2025.

Yang, C., Wang, X., Kang, S., Xu, M., Zhang, Y., Wei, J., and Fu, C.: A Global Perspective on the Development and Application of Glacio-Hydrological Model, 653, 132 797, https://doi.org/10.1016/j.jhydrol.2025.132797, 2025.

Yang, R.: Frontal_ablation_svalbard_SermeQ_PyGEM_OGGM, https://doi.org/10.11582/2026.7WHVAS95, nIRD RDA [Data set], 2026.

Yang, R. and Debolskiy, M.: Frontal ablation Modeling SermeQ-PyGEM-OGGM v0.0.1, https://doi.org/10.5281/zenodo.18761730, zenodo [code], 2026.